Ride Dynamics of General Atomics' Urban Maglev

(*) David W. Doll, (**) Robert D. Blevins, (***) Dilip Bhadra
(*) General Atomics, 3550 General Atomics Court, San Diego, CA 92186, USA,
858 455 3888, david.doll@gat.com,
(**) Consultant, 3818 Pringle St., San Diego, CA 92103, USA
619 297 3827, rdblevins@aol.com
(***) Consultant, 4532 Jutland Place, San Diego, CA 92117, USA
858 272 8233

Keywords

EDS, Maglev, Urban Maglev, LSM, PM

Abstract

The dynamics and ride quality of a new concept in Urban Maglev design have been analyzed. The vehicles utilize permanent magnets (PM) arranged in Halbach arrays for levitation and a linear synchronous motor (LSM) for propulsion. The vehicle was modeled in one-dimension with two degrees-of-freedom (dof) using linear theory. Next, the vehicle was modeled in six dof with MSC/NASTRAN Motion, with the force input into the vehicle programmed to emulate magnetic coupling with the guideway in levitation, drag and propulsion. A control algorithm was incorporated into the propulsion that simulated damping by adjusting the velocity in a feedback loop. All six dof interacted dynamically. The results showed that the vertical accelerations could meet the 8-hour comfort limit set by the International Organization for Standardization (ISO) and that the vehicle could be operated without creating instabilities in any of the six degrees of freedom. Comparison of analytical results with test data awaits construction of a full-scale test track.

1 Background

The Federal Transit Administration (FTA) sponsored Urban Maglev program to develop magnetic levitation technology for urban mass transportation in the United States. One project under this program is managed by General Atomics (GA), San Diego, California. A team of companies and organizations with unique strengths and capabilities suited for developing a maglev system has been assembled to support the effort. A design has resulted that has unique attributes. This new electro-dynamic suspension (EDS) Maglev system utilizes PMs in Halbach arrays for levitation and a LSM for propulsion using Halbach arrays on the vehicle as the salient poles. The vehicle, or train of up to 4 vehicles, is driverless, relies on a fully automatic control of the LSM, and runs on an elevated guideway. Each 12 m long vehicle will carry up to 100 passengers to speeds of 160 km/hr [1].

Because the levitation is via an EDS system, the degrees of motion are coupled magnetically, and can only be analyzed by incorporating the algorithms describing lift and drag into codes that describe the vehicle dynamics. This problem has been approached in two steps. The first was to utilize a one-dimensional 2 degree-of-freedom model of the vehicle that used linear theory and did not address mutual coupling to the remaining degrees of freedom. This facilitated comparison of the results with ISO standards of ride quality. The second analysis utilized the non-linear coupled magnetic relationships governing vehicle levitation, guidance and propulsion of a rigid-body vehicle mass modeled in MSC/NASTRAN Motion [2]. The results of these analyses are reported and discussed.

2 System Design

The system consists of small light-weight vehicles that travel on an elevated guideway. Each vehicle is 12 m long by 2.6 m wide and 3 m tall and weighs 16500 kg fully loaded (Figure 1). The guideway consists of concrete beams-on-columns on which 15 m long track modules are laid and leveled. The

levitation, guidance and propulsion components reside on both sides of these modules leaving the exposed upper surface clear and unobstructed for wheel landings at the stations or between. Levitation comes from the interaction of four sets of magnets, one on each corner of the vehicle, with a ladder-track cantilevered from the box module structure. Each magnet set is made up of upper and lower assemblies of 50 mm Neodymium Iron Boron (NdFeB) cubes (B_r = 4 T, H_{cj} = 15 kOe) arranged in nine 0.4 m long wavelength Halbach arrays. The lower arrays are 0.4 m thick to provide balanced clearances when levitated to a gap of 25 mm. This dual Halbach array arrangement [3] places one set of magnets above and one below a ladder track. The track rungs are 20 mm square copper Litz wire bundles encased in 3 mm thick stainless steel tubes; a copper shorting bar on each side of the rungs closes the conducting loop. The LSM is in line and above the levitation magnets. The iron-teeth that hold the LSM conductors act as the lateral guidance mechanism and provide supplementary lift to the levitation by attraction to the Halbach arrays (salient poles). This amounts to 20% when the vehicle is at rest and 40% when the vehicle is levitated to the nominal 25-mm air gap.

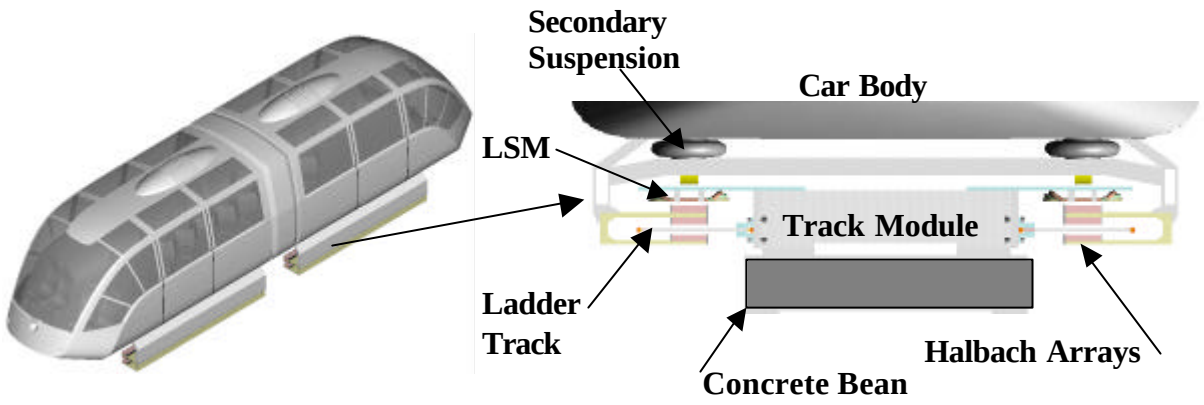

Figure 1. Urban Maglev Vehicle and Guideway

3 Ride Quality

Ride quality has been a major part of the Urban Maglev conceptual design. Criteria for ride quality relate measurements of vehicle behavior to a passenger's subjective evaluation of what is commonly known as Ride Quality. We have adopted the most well known guidelines as published by the ISO [4]. These guidelines relate the RMS acceleration to frequency for three linear degrees of freedom, which are the upper limits with respect to passenger comfort. These guidelines do not necessarily apply to the case where any of the angular degrees of freedom become important.

Motion disturbances could be stochastic, periodic or anomalous. Stochastic disturbances are those due to track irregularities caused by the manufacturing process, installation or wear [5,6]. Periodic inputs include motion due to track deflections between supports; anomalous inputs, as contrasted with steady-state inputs are those, which cause a 'jolt-like' sensation over a short time period. These are deterministic and should be considered in the final suspension design in order to prevent suspension or vehicle damage, if not extreme momentary discomfort. The two major obstacles that stand in the way of making accurate predictions of ride quality are: There has not yet been a prototype vehicle or track built and tested, and there is no way of knowing the irregularities due to construction and installation that must form the basis for the predictions. This leaves only the existing railroad data and the theoretical model used in the transportation industry [7]. In response to this need, a one-dimensional, 2 dof model was used to investigate the effects of track irregularities. The model includes "pad-averaging," which accounts for the distributed nature of the magnetic levitation pads and how they respond to track irregularities. Both a non-linear velocity-dependent magnetic spring and flexible structural supports of the primary suspension are included.

3.1 Analytical Methods

Ride quality is estimated using a 2 dof model and obtaining a transfer function for steady-state disturbances applied to the vehicle motion. The effect of transient disturbances was studied using the Laplace transform applied to the initial value problem. In frequency ? space the power spectral density (PSD) of acceleration becomes

$$a_2^2(\omega) \equiv \omega^4 T^2(\omega)\phi(\omega) \tag{1}$$

where

T(?) = Transfer function of the linear suspension

f(?) = output power spectral density (PSD) for displacement

a_2 (?) = output acceleration response.

The RMS acceleration for the car body is

a_2(?) = output acceleration response

$$= \sqrt{\left| \omega \cdot a_2^2(\omega) \right|}$$

A model used in contemporary railroad design literature [8] attempts to estimate the effect of terrain randomness to provide track profile design criteria. The model essentially defines how to determine necessary terrain alterations such as leveling of hills and filling of depressed areas. The derivation of this model is based on the 'random walk' characteristics of the terrain. One notes the guideway profile between the benchmarks defining the end of a guideway module is modeled as straight, and the benchmarks are spread at intervals of length L. The random variations, δ in the elevation of each consecutive benchmark along the profile are assumed to be independent with a zero mean and a standard deviation of σ. We adopt this model for the case of a track built with conducting sections of length L with an end-to-end random deviation of δ. A vehicle travels over this track at velocity V creating a frequency ω from the spaced irregularities. The equation for the PSD of this constrained 'random walk' model is given by:

$$\phi'(\omega) = \frac{4\sigma^2 V^3}{L^3 \omega^4}\left(1 - \cos(\frac{\omega L}{V})\right) \tag{2}$$

For irregularities much smaller than *L*, the more familiar and conservative correlation of the PSD roughness in terms of the wave number and the characteristic wavelength, $k = 2\pi/\lambda$ is

$$\phi_r(k) \approx \frac{2\sigma^2}{Lk^2} = \frac{A}{k^2} \tag{3}$$

where

$$\omega = kV$$

$$\phi(\omega) = \phi_r(k)\frac{dk}{d\omega} = \frac{AV}{\omega^2} \tag{4}$$

A = roughness parameter

$$A = \frac{2\sigma^2}{L}$$

Early measurements of the PSD identified purely random waveforms, which can be approximated by the above expression (2). Equations (2) and (4) define limits within which the actual response is likely to fall.

A Maglev vehicle is characterized by four significant modes of motion: heave, pitch, roll and sway. For the purpose of preliminary suspension optimization, the heave model was used for this linear analysis. Applying Newton's Law to the bogie mass m_1, carbody mass m_2, spring constants k_1, k_2 and damping coefficients c_1 and c_2, the differential equations describing their motion can be derived. Arranging these in matrix form and solving for the coefficients with subscript 1 denoting the primary suspension and subscript 2 denoting the secondary suspension, a solution is obtained. The equations can then be Laplace transformed and combined to produce any transfer function of interest. For the purpose of this analysis, the displacement transfer function *T(w)* is used. The following identities are defined:

$$\omega_1^2 = \frac{k_1}{m_1} \qquad \beta_1 = \frac{c_1}{2m_1\omega_1} \qquad R = \frac{m_2}{m_1} \tag{5}$$
$$\omega_2^2 = \frac{k_2}{m_2} \qquad \beta_2 = \frac{c_2}{2m_2\omega_2}$$

The displacement transfer function is:

$$T(?) = \frac{\left[1-\left(4\cdot\beta_1\cdot\beta_2\cdot\frac{\omega_2}{\omega_1}\right)\cdot\frac{\omega^2}{\omega_2^2}\right]^2+\left[\left[2\cdot\left(\beta_1\cdot\frac{\omega_2}{\omega_1}+2\cdot\beta_2\right)\right]\cdot\frac{\omega}{\omega_2}\right]^2}{:)\cdot\frac{\omega_2^2}{\omega_1^2}+4\cdot\beta_1\cdot\beta_2\cdot\frac{\omega_2}{\omega_1}\cdot\frac{\omega^2}{\omega_2^2}+\frac{\omega^4}{\omega_1^2\cdot\omega_2^2}\right]^2+\left[\left(2\cdot\beta_1\cdot\frac{\omega_2}{\omega_1}+2\cdot\beta_2\right)\cdot\frac{\omega}{\omega_2}-\left[(1+R)\cdot2\cdot\beta_2\cdot\frac{\omega_2^2}{\omega_1^2}+2\cdot\beta_1\cdot\frac{\omega_2}{\omega_1}\right]\cdot\frac{\omega^3}{\omega_2^3}\right]^2} \tag{6}$$

3.2 "Pad-Averaging"

We refer to the averaging process of a track irregularity over the length of a magnetic pad as "pad-averaging". Averaging over the finite length of the Halbach array pads provides an effective filter for short wavelength irregularities, i.e., where the characteristic spacing is small relative to the pad length. Starting with a model that assumes a finite length pad *Lp* moving over a surface having a sinusoidal roughness, the mean-square roughness was derived and translated into frequency space. The pad-averaging results in a multiplicative factor to *f(w)*:

$$\phi_{PA}(\omega) = \phi(\omega)\left(\frac{2\left(1-\cos\left(\frac{\omega L_P}{V}\right)\right)}{\left(\frac{\omega L_P}{V}\right)^2}\right) \tag{7}$$

3.3 Spring Rates and Damping

Spring rates and damping coefficients were selected to best fit the characteristics of the primary and secondary suspensions. A third degree polynomial was fit to the non-linear primary spring constant derived from the magnetic lift and change in gap. This was combined in series with the spring constants for the cantilever Halbach array support and the Litz wire track in order to arrive at an overall equivalent spring constant, which varied with velocity. No damping ($c_1 = 0$) was assumed for the primary suspension since damping is expected to be small. The secondary suspension spring constant and damping coefficient were established to agree with available or obtainable equipment. Air springs were chosen since they can be adjusted by air pressure to maintain the ride height necessary to align with station platforms; ordinary hydraulic shock absorbers were chosen for damping. A half-full vehicle ($m_2 = 13000$ kg) was selected as the basis for choosing the overall spring constant and damping coefficient. Corrections were included in the calculations that adjusted the spring constant for the pressure variations that will be necessary to adjust the ride height for the range of passenger loads. The best overall fit for damping the vehicle is about 30% . This suppresses the

high frequency primary peak (~11 Hz) without significantly increasing the low frequency secondary peak (~0.9 Hz). The values used in the computations are

$$k_1(20\frac{m}{sec}) = 2.728x10^7\frac{N}{m};\quad c_1 = 0 \qquad \xi = \frac{c}{c_{critical}}$$
$$k_2 = 3.317x10^5\frac{N}{m};\quad c_2 = 2.8x10^4\frac{kg}{sec} \qquad c_{critical} = 2\sqrt{km} \tag{8}$$

4 Results of 1-D 2 dof Analysis

The one dimensional 2 dof model showed the vehicle met the ISO 1 hour ride comfort criteria. A plot of the RMS acceleration in 1/3 octave band center frequencies for a half-full vehicle compared with the ISO standards (upper 4 curves) is given in Figure 2. The upper dynamic response curve represents $f(k) = A/k^2$ (Eq. 3), while the lower dynamic response curve represents the more current correlation (Eq. 2), which accounts for discrete length track modules; an order of magnitude separates them. The 11 Hz resonance peak is characteristic of the primary suspension and the ~1 Hz peak is the secondary suspension response. At the 20 m/sec speed used in the calculations, the effect of zero damping in the primary is overshadowed by the damping between the primary and secondary. This is a potential advantage of the Urban Maglev systems. Higher speeds still need to be evaluated.

Pad averaging is the most significant contributor to the low accelerations predicted. Calculations not including this effect (i.e., steel wheels on steel rails) were an order of magnitude higher placing the peak acceleration above the 1-hour ISO limit. This is to be expected since irregularities spaced less than 3.6 m would increasingly be averaged. A full vehicle (16500 kg) would have even a smoother ride. This is for the obvious reason that the resonant frequency would go down and the roughness would have less effect on the car body acceleration. Conversely, the ride quality for an empty vehicle (9500 kg) would be worse because more of the high frequencies would get through to the car body.

The conclusion is that with our baseline design track irregularity of ±3 mm at the joints between guideway modules (15 m length), our vehicle will be well below the ISO 1 hour ride quality standard.

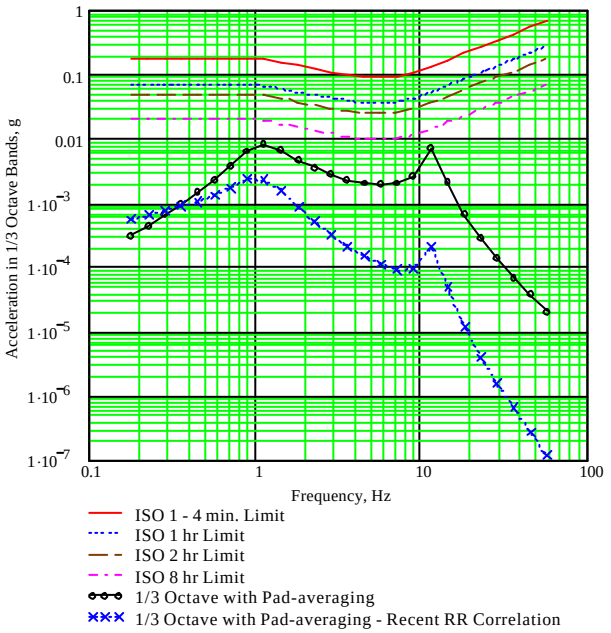

Figure 2. Dynamic Response in 1/3 Octave Bands of a Vehicle with Fifty Passengers. Analysis Used Two Roughness Models with Pad Averaging. Comparison is Made with ISO Standards.

5 Vehicle Dynamics

The dynamic stability of the vehicle was characterized using both analytical and numerical methods. First, the Hurwitz Stability Criterion [9] was applied to the dynamic force equations and the limits of stability defined. Second, the forces on a rigid vehicle were defined. For the levitation, the lift and drag forces were defined in terms of the geometry, magnetic parameters and velocity. For guidance, which is an attractive force between the LSM Halbach array and the iron supports, an algorithm derived from a curve-fit describing the force was used. For propulsion, a force was applied to the vehicle at the locations they occupy on the primary suspension above the levitating magnets. This force was modulated through an algorithm that simulated a feedback control on the velocity. Methods for performing these calculations are described. The vehicle and LSM were simulated numerically with a six dof NASTRAN model.

5.1 Forces Acting on Vehicle

To model motion in the forward direction, it was necessary to develop expressions for forces in the forward direction and determine how they vary with both gap and velocity. This was done analytically for the double Halbach array magnetics model (Figure 3).

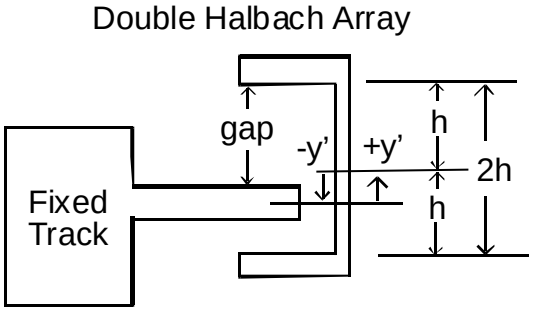

Figure 3. Definitions of magnetic geometry

The forces acting on the vehicle can be shown [3] to be:

$$F_{lift} = \frac{a A_{fp}}{L}\frac{f}{c}\frac{e^{-2kh}}{2k^3 d_{tr}^2}\left(e^{2kd_{tr}}-1\right)^2 [\, B_{01}^2 e^{2k(y'-d_{tr})} - B_{02}^2 e^{-2k(y'+d_{tr})}\,]\frac{1}{1+(v_t/v)^2} \qquad (9)$$

$$F_{drag} = \frac{a A_{fp}}{L}\frac{f}{c}\frac{e^{-2kh}}{2k^3 d_{tr}^2}(e^{-2kd_{tr}}-1)^2 [\, B_{01} e^{k(y'-d_{tr})} - B_{02} e^{-k(y'+d_{tr})}\,]^2 \frac{v_t/v}{1+(v_t/v)^2} \qquad (10)$$

where

a = width of Halbach array = 0.25 m
A_{fp} = footprint area of the entire double Halbach array = 2.19 m
L= inductance of λ/2 piece of tract = 0.24×10^{-6} Henry
R = track loop resistance = 1.92×10^{-5} O
f = filling factor of rungs = 0.5, dimensionless
c = width of one rung in x-direction =0.02 m
d_{tr}=track half thickness =0.010 m
h=half gap between the two arrays=0.035 m
k = wave number = $2\pi/\lambda$=15.708 cycles/m
λ= magnetic wave length = 0.4 m
v_t= transition velocity = $\lambda/(2\pi\tau)$ = 5.305 m/s
τ = L/R =0.0125 sec
ω = $2\pi v/\tau$

B_{01} = field at magnet surface =0.689 Tesla
B_{02} = field at magnetic surface =0.591 Tesla
y' = h-y
t = time
v= dx/dt, longitudinal velocity, positive forward
x = longitudinal position of the car, also called surge displacement
y = vertical gap, also called heave displacement
y' = h-gap.

The lateral force due the LSM is given by a curve fit to an analytical solution of the attractive forces where z is lateral distance from the vehicle centerline.

$$F_{lateral} = 1.53E6z - 8.89E8z^3 + 1.412E11z^5 \tag{11}$$

Further, there is a component of lift generated by attraction to the LSM given by

$$F_{lift-synchmotor} = -4.87E7z^2 + 1.087E10z^4 \tag{12}$$

Lift and drag are coupled though velocity and vertical position; the other degrees of freedom couple though the mechanics of the vehicle suspension.

5.2 Analytical Test for Stability

The dynamic stability of the vehicle for motions in the coupled x and y directions was tested using the Hurwitz Stability Criterion. This simple method uses the fact that coefficients of a third degree polynomial formed by the differential equation coefficient matrices must be positive to be stable. Applying Newton's laws to the vertical and forward motion the net forces can be written. Since the drag and motor force sum in x direction, and the lift force and weight Mg sum in the y direction, two new total forces are defined as the net longitudinal drag and net lift.

$$F_x = F_{drag}(v,y) - F_m \tag{13}$$
$$F_y = F_{lift}(v,y) - Mg \tag{14}$$

Expanding equations (15) and (16) in first order Taylor series gives:

$$M\frac{d^2x}{dt^2} = -F_x(v_o, y_o) - \frac{\partial F_x}{\partial v}dv - \frac{\partial F_x}{\partial y}dy \tag{15}$$
$$M\frac{d^2y}{dt^2} = F_y(v_o, y_o) + \frac{\partial F_y}{\partial v}dv + \frac{\partial F_y}{\partial y}dy \tag{16}$$

Consider the stability of small perturbations assumed to grow as e^{at} about the steady equilibrium solution for the gap = y_o, and forward velocity =v_o.

$$v = v_o + dv = v_o + v_1 e^{\alpha t}, \quad \text{where } v_1 << v_o, \tag{17}$$
$$y = y_o + dy = y_o + y_1 e^{\alpha t} \quad y_1 << y_o \tag{18}$$

The Hurwitz Stability Criterion can now be applied. Setting the determinant of the matrix on the left hand side of the coefficient matrix to zero gives the following polynomial:

$$\alpha^3 + \alpha^2 \frac{1}{M}\frac{\partial F_x}{\partial v} - \alpha \frac{1}{M}\frac{\partial F_y}{\partial y} - \frac{1}{M^2}\frac{\partial F_x}{\partial v}\frac{\partial F_y}{\partial y} + \frac{1}{M^2}\frac{\partial F_x}{\partial y}\frac{\partial F_y}{\partial v} = 0 \qquad (19)$$

which is then solved for α . The results show that the stability criteria are not met for the vehicle with a constant thrust force. An instability will be driven by the decrease in drag with increasing velocity and its interaction with lift at particular points of operation unless velocity dependent control forces are applied.

$$\frac{\partial F_{drag}}{\partial v} > \frac{\partial F_{motor}}{\partial v} \quad \text{for stability.} \qquad (20)$$

The net system is stable if the LSM control is sufficiently stabilizing. That is, the LSM force must decrease as the desired speed is approached from a lower velocity faster than the drag reduces.

5.3 Six dof Numerical Simulation

The MSC/NASTRAN Motion model of the vehicle consisted of two halves joined by an articulated joint as shown in Figure 4. The vehicle itself is modeled as a body volume, which is supported by a spring and link suspension from a rigid magnetic frame that carries magnetic pads. The secondary suspension consists of a 3 bar linkage and four springs and dampers located at the corners. The weight distribution used was 6800 kg for the car-body, 4840 kg for the car-body base and 4860 for the levitation primary for a total of 16500 kg.

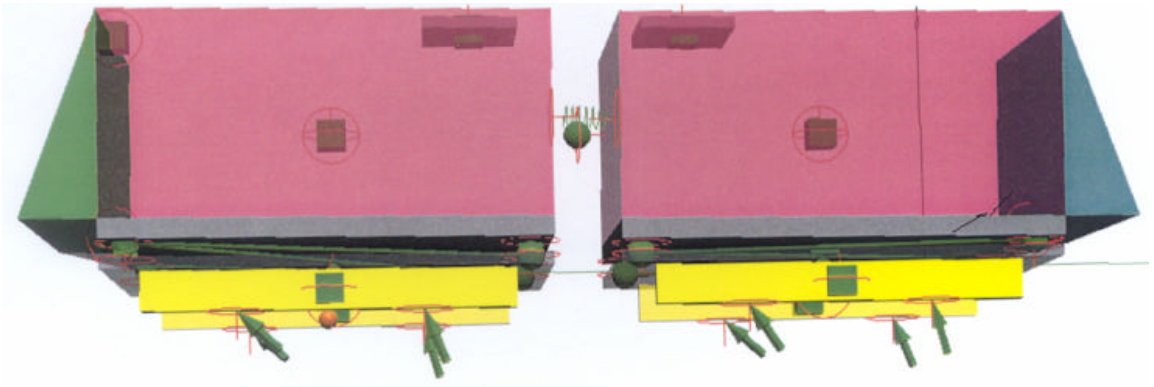

Figure 4. NASTRAN 6 dof model used in numerical simulation. The arrows at bottom are the magnetic forces applied to the model. An articulated joint connects the two haves of the vehicle. The model is accelerating right to left.

The spring rates of the secondary suspension springs are 57600 N/m each and the damping is 5500 kg/s each, which gives a nominal natural frequency of 1 Hz and 30% damping to the car body, the same as for the one dimensional model. The magnetic forces were applied to 2 points spaced at points 1/3 and 2/3 along each of the two magnetic pads. This simulated the distribution of the magnetic loads. One eighth of the total forces cited earlier in this section were applied to each of the four points for the half vehicle model. The model was used to simulate the take-off and cruise of the vehicle without any external restraint other than the magnetic forces and gravity. The simulation works by simultaneously numerically integrating in time the 6 dof motions. No degrees of freedom were removed or artificially restricted.

The longitudinal thrust from the LSM is a linear function of velocity with constants a and b whose selection determine the stability of the vehicle.

$$F_{synmotor} = a(x_{desired} - x_{current}) + b(v_{desired} - v_{actual}) \quad (21)$$

The symbol x refers to distance down the track and v=dx/dt is velocity along the track. The simulation is started on wheels until the magnetics provide sufficient lift and remains levitated as long as the velocity is maintained. In a simulated lift-off, the vehicle is dropped slightly onto the wheels at time zero. Then the model control, x-desired and v-desired, is requested to accelerate at the desired rate of 1 m/sec^2 with a = 0.5 E6 N/m. Two forms of motor damping were used. First, b=0, corresponding to no motor damping, and second, b=20000 N/m/sec representing strong motor damping. Instantaneously requesting a 1 m/sec^2 acceleration causes the synchronous motor to rock back on its control logic until sufficient force is developed that the vehicle achieves the desired acceleration.

5.4 Results of 6 dof Simulation

The simulation confirmed the predictions made using the Hurwitz stability criterion (Section 5.2), namely that feedback control was required on the velocity in order to control oscillations. Figure 5 shows the drag build up as the vehicle increases velocity but is still on its wheels. At the point where the vehicle comes into equilibrium with the velocity determined gap, it follows a declining drag force with increasing velocity. It is in this region that oscillations can occur. Figure 6 shows the movement at the center of the passenger cabin during take off with and without motor damping. Without motor damping, while oscillations develop in the longitudinal (x) direction that spreads to the vertical (z) direction, no growth instabilities are observed. With damping, the oscillations are suppressed, except for some initial 'kick' at takeoff.

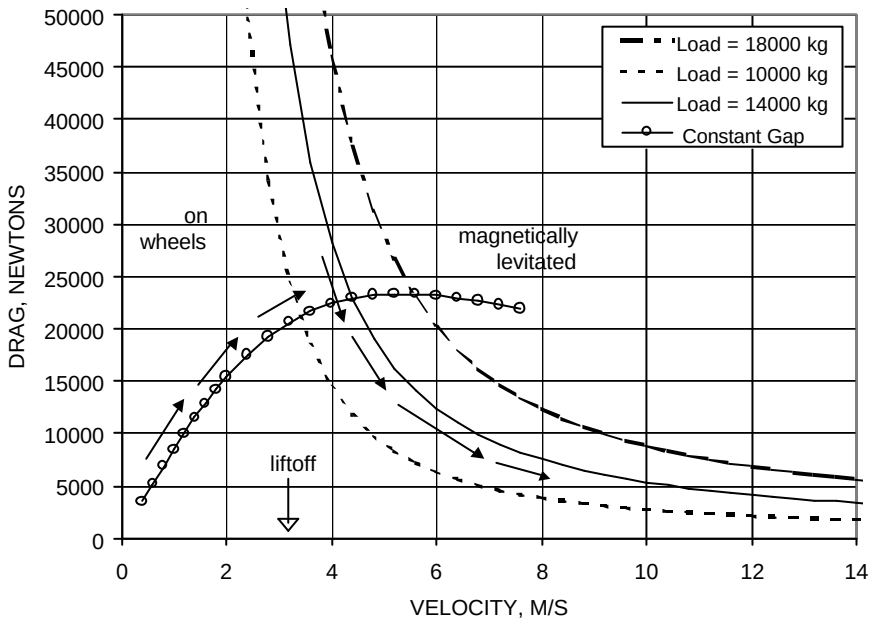

Figure 5. Lift as a function of velocity for the double Halbach array at three vertical positions relative to the track.

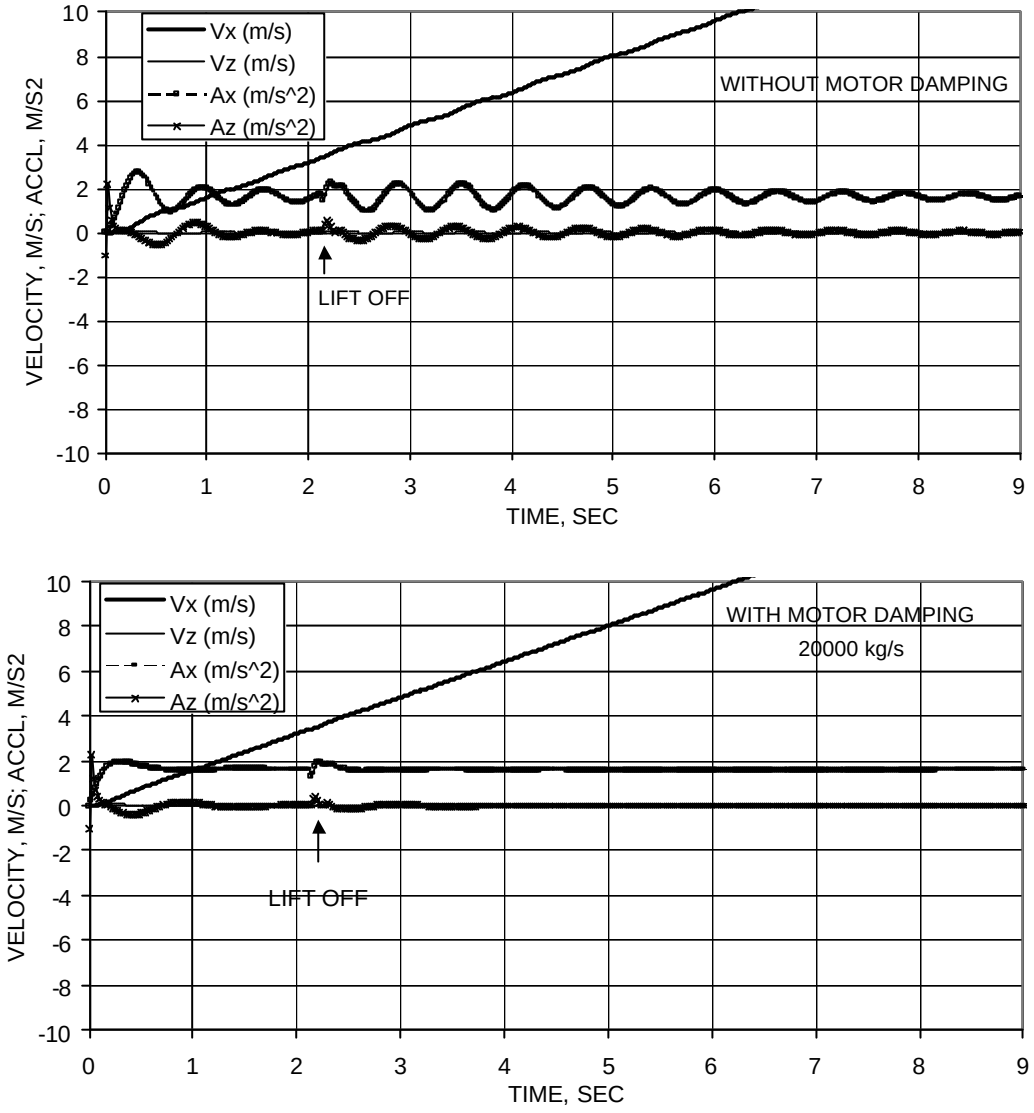

Figure 6. Position of passenger cabin versus time for acceleration at 1 m/s^2 from stop to 9 m/sec with and without synchronous motor damping. Z is vertical and X is longitudinal. Vx is longitudinal velocity and Ax is longitudinal acceleration. Lift off wheels occurs at about 2.9 sec.

6 Conclusions

The ride quality of the vehicle will meet or exceed that required by ISO. This is due primarily to the averaging effect of long ski-like levitation pads. Adaptive damping in the secondary suspension is not necessary for speeds of interest. LSM control is found to be very effective in providing damping control of induced oscillations. A six dof simulation of the vehicle driven by the operational control logic is necessary to validate many of the conclusions drawn. This work is part of the scheduled system development to be completed prior to test track demonstrations, which will ultimately validate the models used.

7 Acknowledgements

This paper presents the results of a research effort undertaken by General Atomics under Cooperative Agreement No. CA-26-7025 to the Office of Research, Demonstration, and Innovation, Federal Transit Administration.

8 References

1. Sam Gurol, Bob Baldi, and Richard L. Post, "Overview of the General Atomics Urban Maglev Program," Maglev 2002, Lausanne, Switzerland, September 4–8, 2002
2. MSCVISUAL NASTRAN, version 6.2, MSC software, Los Angeles, CA, 2000
3. R. Kratz and R. Post, "Null-Current Magnetic Suspension System, International Symposium on Magnetic Suspension Technology, Turin, Italy, October 7 – 11, 2001
4. International Organization for Standardization, ISO 2631-1 1997 and ISO 2631, 1985
5. J.H. Ragazzini and G.F. Franklin, *Sample-Data Control Systems*, McGraw-Hill, NY (1958).
6. J.L. Melsa and A.P. Sago, *An Introduction to Probability and Stochastic Processes*, Prentice Hall (1973).
7. B.J. Brock, "Determination of Guideway Roughness from Construction Tolerances", *Proc. Of 44th Shock and Vibration Symposium.* (1973).
8. D.A. Hullender and T.M. Bartley, "Guideway Roughness as Related to Design Tolerances and Profile Constraints" (1974) Urban Mass Transportation Report.
9. Richard Bellman, *Introduction to Matrix Analysis*, 1997, 2nd ed., McGraw-Hill-N.Y., 1970, p. 253.